

International Journal of Modern Physics E
© World Scientific Publishing Company

FUSION INDUCED BY RADIOACTIVE ION BEAMS

J. F. Liang

*Physics Division, Oak Ridge National Laboratory
Oak Ridge, Tennessee 37830, U.S.A.
liang@mail.phy.ornl.gov*

C. Signorini

*Physics Department of the University and INFN,
via Marzolo 8, 35120 Padova, Italy
cosimo.signorini@pd.infn.it*

Received (received date)

Revised (revised date)

The use of radioactive beams opens a new frontier for fusion studies. The coupling to the continuum can be explored with very loosely bound nuclei. Experiments were performed with beams of nuclei at or near the proton and neutron drip-lines to measure fusion and associated reactions in the vicinity of the Coulomb barrier. In addition, the fusion yield is predicted to be enhanced in reactions involving very neutron-rich unstable nuclei. Experimental measurements were carried out to investigate if it is feasible to use such beams to produce new heavy elements. The current status of these experimental activities is given in this review.

1. Introduction

The interaction of two nuclei consists of a repulsive Coulomb potential and an attractive nuclear potential. The overlap of the two potentials produces a Coulomb barrier. Fusion occurs when the interacting nuclei have sufficient kinetic energy to overcome the repulsive barrier and are subsequently trapped inside the potential pocket to form a compound nucleus. The kinetic energy determines whether the process takes place by going over or quantum tunneling through the barrier. The nucleons in the reactants are rearranged in the compound nucleus.

Nuclear fusion is responsible for energy generation in stars. It is also a process for synthesizing new elements in laboratories. The study of fusion has been carried out for several decades. In the 1980s, the discovery of unexpectedly large fusion cross sections at sub-barrier energies in some heavy-ion systems generated tremendous interest in fusion studies.^{1,2,3} The sub-barrier fusion enhancement can be understood in the coupled-channel formalism.^{4,5} The coupling of the entrance channel to the intrinsic degrees of freedom of the projectile and target splits the uncoupled single barrier into a distribution of barriers. The enhanced fusion cross

sections at sub-barrier energies arise from going over the low energy barriers.

The advent of radioactive ion beams (RIBs) has generated new excitement in this field. The r.m.s. radius of nuclei far from the β -stability valley is, in many cases, significantly larger. Fusion is expected to be enhanced due to lower barriers. However, these nuclei are often loosely bound, *i.e.*, the valence nucleon(s) have very small binding energy. Breakup of the loosely bound nuclei in the Coulomb and/or nuclear field of the target can take place and thus remove the available flux for fusion. As a result, fusion is predicted to be suppressed.^{6,7} On the other hand, if breakup is significantly large fusion can be enhanced through the strong coupling.⁸ How fusion is influenced by loosely bound nuclei is still an open question, as will be seen later in this review.

Several stable beam experiments have showed that neutron transfer with positive Q-values can enhance sub-barrier fusion.^{9,10,11,12,13} With neutron-rich radioactive beams, the number of transfer channels with positive Q-values can be very large. One would expect an enhancement of sub-barrier fusion by the coupling to these transfer reactions.^{14,15} The compound nucleus formed with neutron-rich radioactive nuclei induced reactions should have higher stability against fission. Using short-lived neutron-rich radioactive beams may be a viable way for producing new heavy elements.¹⁶ Results of fusion measurements performed with some low intensity neutron-rich radioactive beams will be discussed in this paper.

The emphasis of this review is on experimental work. General discussions on recent theoretical developments in fusion can be found in review articles by Balantekin and Takigawa,⁴ Dasgupta *et al.*,⁵ and Signorini¹⁷. However, specific theoretical treatments on some of the measurements discussed will be presented where the experiment is mentioned. The challenges in conducting fusion measurements with radioactive beams will be shown in Sect. 2 followed by a brief description of techniques for producing radioactive beams. Measurements using light-mass and medium-mass radioactive beams will be discussed in Sect. 4 and Sect. 5, respectively. Concluding remarks will be given in Sect. 6.

2. Experimental Considerations

Fusion is commonly studied by measuring the cross section as a function of reaction energy. The cross section can be determined by detecting the evaporation residues or fission fragments directly, or by detecting the γ rays or light particles emitted from the evaporation residues deposited in a catcher foil. The techniques used in radioactive beam measurements are similar to those used in stable beam experiments.^{1,2}

It is very important to have high quality beams for fusion measurements. Good energy resolution, small energy width, is crucial for measuring excitation functions, particularly at energies below the barrier where the cross sections change exponentially. To determine whether sub-barrier fusion is enhanced the reaction energies have to be known better than $\sim 1\%$. Low emittance beams which result in a beam

spot of a few mm on target are desirable. This reduces the angular broadening and energy spread of the reaction products. Beam purity is often an issue in RIBs, and it is associated with the production processes. The unwanted contaminants can be removed or reduced by high resolution mass separators or chemical methods. But sometimes they cannot be completely eliminated because the beam of interest is orders of magnitude less intense than the contaminants. Therefore, measurements with the main contaminant beam species have to be performed and subtracted from measurements with the mixed beam.

The intensity of RIBs is, presently, several orders of magnitude lower than that of stable beams. In stable beam experiments, the beam intensity can be measured by a Faraday cup. One particle nA is 6.24×10^9 particles per second (pps). In RIB experiments, an intensity of 10^6 to 10^7 pps would be considered high today. Fusion measurements can be performed with a beam of 10^4 pps. In order to compensate for the low beam intensity, high efficiency detectors with large solid angle coverage or multiple targets for obtaining measurements of several energies in one run have been employed. The availability of large area silicon strip detectors (SSD) in a variety shapes and compact multichannel electronics for handling such detectors have made many measurements feasible. On the other hand, because of the low beam intensity, the use of event-by-event beam tracking is very useful for cleaning up events originating from contaminant induced reactions. Incorporating time-of-flight measurements into experiments has many advantages and is very common. It can be used to measure beam energies. When beam contaminants are present, valid events can be selected using timing gates corresponding to the correct beam particles. The decay of beam particles sometimes contributes to the background in detectors. With the use of time-of-flight, this background can be suppressed effectively.

3. Types of Radioactive Ion Beams

The production of RIBs has been discussed extensively in many reports¹⁸ and is beyond the scope of this review. We will give a brief description of the methods used to produce beams for the experiments discussed in this paper.

3.1. *Isotope separator on-line*

The isotope separator on-line (ISOL) method uses a driver accelerator to accelerate light-charged particles, such as protons, deuterons, and α particles, into a thick target.^{19,20,21} The radioactive atoms diffuse out of the target and get ionized in an ion source. The secondary ions are then selected by mass separators, accelerated by a post accelerator, and sent to an experimental area, as shown in Fig. 1(a). The beam quality is very good because the post accelerator is usually an electrostatic tandem accelerator or a linac. Beams which can be produced with this method are limited to those with lifetimes of the order of seconds or longer. Species with shorter lifetimes may not be able to get out of the target fast enough for post acceleration.

How fast a radioactive atom gets out of the target depends strongly on the chemical and structural properties of the target.

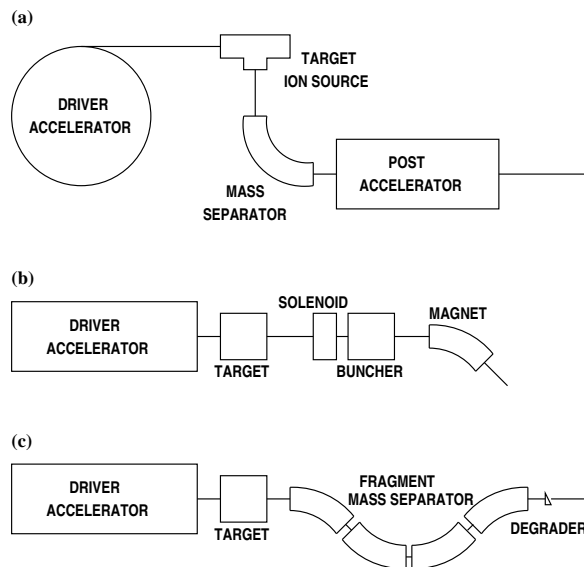


Fig. 1. A schematic illustration of RIB production: (a) ISOL, (b) in-flight with direct reactions, and (c) in-flight with fragmentation reactions.

3.2. *In-flight*

In this method, radioactive beams can be produced with the use of one accelerator. The accelerated heavy-ion beam is incident on a thin target in inverse kinematics. The reaction products emitted in a narrow cone in the forward direction are focused and transported through mass separators. At energies near and below 10 MeV/nucleon, direct reactions are often used. The reaction products can be selected and focused by solenoids such as the TWINSOL facility at the University of Notre Dame,^{22,23} or by a combination of solenoid, bunching resonator, and bending magnet such as at ATLAS (Argonne National Laboratory).²⁴ Figure 1(b) depicts the beam selection by the latter method. At energies of a few tens to several hundreds MeV/nucleon, the production reaction is essentially fragmentation. Very sophisticated fragment mass separators such as the A1900 at NSCL (Michigan State University)²⁵ and RIPS at RIKEN²⁶, is used for filtering the beam, as shown in Fig. 1(c). The advantage of the in-flight production method is that very short-lived species can be produced because diffusion and target chemistry are not involved in the processes. However, reaction mechanisms and target thickness introduces significant energy and angular spreads resulting in poor energy resolution and large emittance of the secondary beam.

4. Light-ion Reactions

This section will discuss the fusion reactions induced by light-mass radioactive ion beams namely, ${}^6,8\text{He}$, ${}^{11}\text{Be}$, ${}^{11}\text{C}$, and ${}^{17}\text{F}$ up to now, which are the only projectiles utilized for this type of study. The ${}^6,8\text{He}$, ${}^{11}\text{Be}$, and ${}^{17}\text{F}$ projectiles are particularly interesting for the following reasons:

- a) ${}^6\text{He}$ is weakly bound with a two-neutron separation energy $S_{2n} = 0.972$ MeV and has a neutron skin like structure with a large neutron spatial distribution around the ${}^4\text{He}$ core.^{27,28} In the present literature ${}^6\text{He}$ is considered as a neutron halo nucleus. The isotope ${}^8\text{He}$ is more tightly bound with $S_{2n} = 2.468$ MeV but still has a structure similar to ${}^6\text{He}$.^{27,28}
- b) ${}^{11}\text{Be}$ is weakly bound, with $S_n = 0.504$ MeV, and has a well established neutron halo^{29,30} which produces a r.m.s. radius $\sim 10\%$ larger than what is expected from the $r_0 A^{1/3}$ systematics with $r_0 \sim 1.18$ fm.
- c) ${}^{17}\text{F}$ is a proton drip-line nucleus with a proton separation energy $S_p = 0.600$ MeV. Its first excited state is bound by 0.105 MeV with an extended r.m.s. radius $r_{rms} = 5.3$ fm which is considered as a halo state.³¹

In addition to the fusion process, the main topics of this review, discussion also includes the breakup (BU) process which is expected to be strong because of the small binding energy of these short-lived nuclei. Such a process could hinder or enhance the fusion process around the barrier as extensively debated by many theoreticians, and/or increase the total reaction cross section.

In the following subsections the experimental results obtained with the light RIBs mentioned above will be critically reviewed as well as the theories developed to explain the measurements. Concerning fusion with loosely bound projectiles, which break up easily, we have to distinguish between the following processes: a) *complete fusion* (CF), when all projectile nucleons are trapped inside the target, b) *incomplete fusion* (ICF), when only part of the nucleons are trapped, and c) *total fusion* (TF), the combination of complete and incomplete fusion cross. In the absence of incomplete fusion, total fusion and complete fusion are identical.

We should bear in mind that theories usually calculate total fusion cross sections, while various fusion cross sections measured by particular experiments. In order to compare different systems, the fusion cross sections should be corrected for geometric factors originating from the different nuclear radii involved, and the energies of the colliding systems (usually the center of mass energies) should be divided by the Coulomb barrier energies, V_B . In the following, V_B will be evaluated with $r_0 = 1.56$ fm. This value was deduced from the barrier distribution for the system ${}^9\text{Be}+{}^{209}\text{Bi}$ (${}^{208}\text{Pb}$) in Ref. ^{32,33} with the standard formula $V_B = Z_p Z_t e^2 / r_0 (A_p^{1/3} + A_t^{1/3})$ for $V_B = 38.50$ (37.75) MeV.

In connection with loosely bound nucleus induced fusion, there is a relevant process where the valence nucleon of the projectile, such as the proton in ${}^{17}\text{F}$, is captured by the target. Such a process can be a conventional transfer/stripping and

will be called “transfer”, or a strong capture/transfer/stripping breakup and will be called “transfer/stripping-breakup”.

4.1. ${}^6,8\text{He}$ beams

The ${}^6\text{He}$ beam is becoming fairly popular. It has been produced in several laboratories by both ISOL and in-flight techniques for fusion studies. For the production of these beams, the ISOL technique has been utilized at the pioneering facility of the Cyclotron Research Centre in Louvain la Neuve (Belgium)²¹ and at the new facility SPIRAL in GANIL (France)²⁰. The in-flight technique has been adopted at the TWINSOL facility at the University of Notre Dame (USA).^{22,23}

4.1.1. *The ${}^6\text{He}+{}^{209}\text{Bi}$ system*

This system, with $V_B = 19.76$ (20.33) MeV in the center of mass (laboratory), has been studied extensively at Notre Dame. The ${}^6\text{He}$ beam is produced by the ${}^9\text{Be}({}^7\text{Li}, {}^6\text{He})$ proton transfer reaction with the following characteristics: intensity $\sim 10^5$ pps, energy ranging from 14 to 22 MeV, energy resolution ~ 1.5 MeV, beam size on target from 5 to 8 mm diameter. The fusion cross section was evaluated by the sum of the $({}^6\text{He}, 3n){}^{212}\text{At}$ and $({}^6\text{He}, 4n){}^{211}\text{At}$ evaporation channels.³⁴ These data are essentially for complete fusion. This cross section could be somewhat underestimated at the lowest energies since the 2n channel, expected to be small, was not studied. The possible incomplete fusion of ${}^4\text{He}$, produced by ${}^6\text{He}$ breakup, and the subsequent 1n emission to ${}^{212}\text{At}$ was excluded by the authors by reaction Q-value arguments. This should eventually be verified experimentally. Within the present results, since there is no incomplete fusion, the complete fusion measured has to be considered as total fusion. This system, compared to ${}^4\text{He}+{}^{209}\text{Bi}$, shows moderate enhancement only in the sub-barrier region as shown in Fig. 2

Above the barrier, the two cross sections, once corrected for the different projectile radii and Coulomb barrier energies, are essentially equal. This suggests that, in this case, the breakup effects have negligible or no influence on the fusion process above the barrier. The breakup process is quite relevant in this system. Indeed, the so-called inclusive α production has been found very strong³⁵ as compared to fusion, particularly below the barrier. This α production is most likely originating from the ${}^6\text{He}$ breakup. This seems to be the only relevant process in addition to the fusion. As a matter of fact, breakup and fusion exhaust the total reaction cross section inferred from the elastic scattering data³⁶, as shown in Fig. 3.

The detailed mechanism of the inclusive α production is not yet very clear. These inclusive α 's can originate by several processes, namely: $\alpha+n+n+{}^{209}\text{Bi}$, $\alpha+n+(n+{}^{209}\text{Bi})$, and $\alpha+(2n+{}^{209}\text{Bi})$. With parenthesis we indicate the nucleus where one or two neutrons are trapped into the target by the nuclear potential. These two processes are of the transfer/stripping-breakup type since they have a cross section much larger than a conventional transfer process, usually

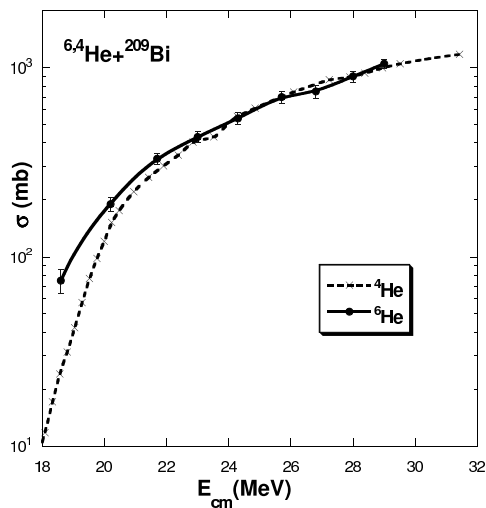


Fig. 2. Fusion cross sections for the systems $^{4,6}\text{He}+^{209}\text{Bi}$. The ^4He cross sections have been corrected for the different radius and Coulomb barrier with respect to the ^6He projectile.

well predicted by direct reaction formalism like distorted-wave Born approximation (DWBA) or coupled-channels.

Very recently α -n coincidence measurements were undertaken by the same Notre Dame group at 23 MeV, slightly above the Coulomb barrier. In their first experiment³⁷, they studied the $^{209}\text{Bi}(^6\text{He},^5\text{He})^{210}\text{Bi}$ reaction followed by $^5\text{He} \rightarrow ^4\text{He}+n$ by measuring the α particle and neutron in coincidence. The neutrons were detected in liquid scintillators with a relatively high threshold (> 1 MeV). The experimental results give evidence that the coincidence events, assigned to one neutron transfer/stripping-breakup, account for approximately 20% of the inclusive α -particle yield which has a cross section of 800 mb.

In their second experiment,³⁸ they studied $^{209}\text{Bi}(^6\text{He},^4\text{He})^{211}\text{Bi}$ by detecting α particles at and beyond the grazing angle in coincidence with neutrons evaporated from ^{211}Bi . The neutrons were detected in solid plastic scintillators with a lower threshold (>0.3 MeV), but unfortunately with a high background of around 45% of the total neutron yield. In this case, such coincidence yield accounts for about 55% of the inclusive α -particle yield. The remaining 25% yield, around 200 mb, of

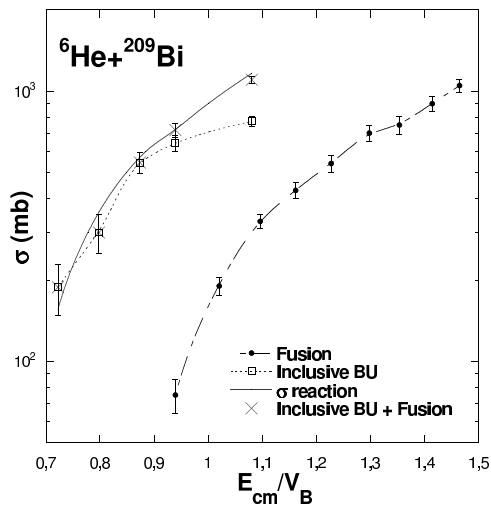


Fig. 3. Cross sections for the following processes in the system ${}^6\text{He}+{}^{209}\text{Bi}$: total reaction (solid curve), total fusion (solid circles), inclusive α production or inclusive breakup (open squares), total fusion+inclusive breakup (crosses). The total fusion+inclusive breakup cross section exhausts the total reaction cross section in the region where common data exist.

the α -particle inclusive events is assumed to originate from a breakup process with all ${}^6\text{He}$ fragments, α and two neutrons, in the exit channel.

These results have similarity to the ${}^6\text{Li}+{}^{208}\text{Pb}$ reaction³⁹. Lithium-6 with $S_\alpha = 1.47$ MeV is the least bound stable nucleus. In this system, strong inclusive α production was observed. The breakup process, α -d as well as α -p coincidences, is approximately one order of magnitude smaller with cross sections ranging from 65 mb to 110 mb around the barrier.

These results make the theoretical description of the ${}^6\text{He}+{}^{209}\text{Bi}$ reaction dynamics quite intriguing, since in addition to the usual coupling to the target or projectile bound state excitations and their consequent barrier distributions, one has to consider also the coupling to the breakup channels, which proceeds in most cases via continuum excitations since they lie above the particle emission threshold.

Several theoretical approaches have been undertaken. A first attempt was done in Ref. ⁴⁰. These calculations (TH1) were done via the coupled-channel formalism

using the ECIS code⁴¹. The real potential was calculated with a double folding model using the BMD3Y1 interaction⁴². The imaginary potential had a small radius in order to absorb all the flux penetrating the barrier simulating the incoming wave boundary conditions. However the real potential had to be reduced by a factor of 0.4 to reproduce the data. This renormalization most likely takes care of the breakup process in a bulk way. In Ref. ⁴³, two other approaches were followed. In the first one, the calculations (TH2) were done with the coupled discretized continuum channel (CDCC) formalism and two slightly different ways of handling the potentials: a) empirical cluster-target optical potentials, and b) short-ranged imaginary parts. In these cases, the code FRESKO⁴⁴ was utilized. The results of the CDCC b) approach, a slightly better one in our opinion, are shown in the Fig. 4. In the second one, calculation (TH3) was done with the barrier penetration model. In this case the potential was parameterized as $V_{nucl} = V_{bare} + V_{pol}$, and the polarization potential was derived from the previous CDCC approach. In TH2 the breakup process is automatically included in the CDCC formalism. In TH3 the breakup enters via the polarization potential V_{pol} . See Ref. ⁴³ for more details. The results of these three different approaches are shown in the Fig. 4.

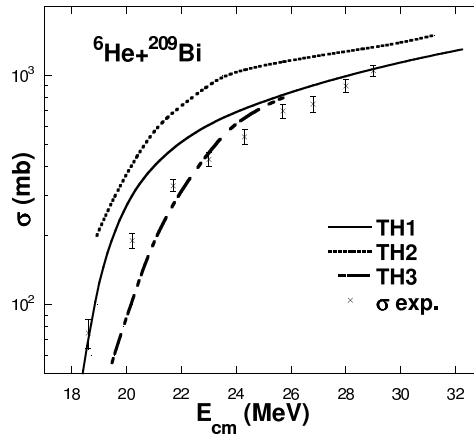


Fig. 4. Theoretical calculations of the ${}^6\text{He}+{}^{209}\text{Bi}$ fusion excitation function. See text for details.

From the inspection of Fig. 4 we see that TH3 and TH1 seem to reproduce the experimental data better, however, not all the points. These two approaches are more phenomenological. TH2 is more fundamental since it is based on the CDCC formalism and reproduces well the elastic scattering as discussed in Ref. ⁴³ but fails as a good reproduction of the fusion. This last problem seems to be, for the moment, always present in this type of approach as we will discuss later in connection with the ${}^6\text{He}+{}^{64}\text{Zn}$ system. However, it should be emphasized that the variation of these

various theoretical predictions is not necessarily bad. It simply demonstrates the evolution and the present status of the theoretical efforts and indicates that, most likely, additional work is needed to evaluate the interaction of loosely bound nuclei at the barrier.

4.1.2. *The ${}^6\text{He}+{}^{238}\text{U}$ system*

This system, with $V_B = 21.19$ (21.73) MeV in the center of mass (laboratory), has been measured twice at Louvain la Neuve. The ${}^6\text{He}$ beam was produced via the ISOL²¹ method with energy resolution $\sim 0.5\%$ and intensity $< 5 \times 10^7$ pps. The first series of measurements was performed at eight energies from 14.6 to 28.7 MeV with four primary energies and four degraded energies using mylar absorbers.⁴⁵ The fusion process was identified by the fission channel. The fission fragments were measured with a large solid angle detection system consisting of large area silicon surface barrier detectors arranged around the target in a box-like structure. In this first measurement, the fission fragments originating from ${}^6\text{He}$ induced fusion, ${}^4\text{He}$ induced fusion, and 1n or 2n transfer/stripping-breakup could not be distinguished, so these results overestimate the total fusion cross section.

As discussed in several papers, the total fusion cross section for ${}^6\text{He}+{}^{238}\text{U}$, identified by all the fission events, is much larger, especially below the barrier, than that for ${}^4\text{He}+{}^{238}\text{U}$ by up to two orders of magnitude. The second experiment⁴⁶ was set up in order to also measure the α -fission fragment coincidences. In this way it was possible to distinguish the fission events originating from total fusion (not in coincidence with α particles) from fission events originating from 1n or 2n transfer/stripping-breakup. Figure 5 presents the results of the two experiments as well as the cross sections with ${}^4\text{He}$ beam for comparison. First of all, it should be noted that at some energies the cross sections measured in the two runs differ well beyond the statistical errors; see, for example, the lowest energy point. In our opinion, this could originate from systematic errors due to the low beam intensity and the related problems of correctly identifying the reaction channel. The most interesting result is, however, that fission below the barrier is only in coincidence with α particles and consequently it originates by transfer/stripping-breakup. Such a process should not be included in incomplete fusion. This result is very similar to that of the ${}^6\text{He}+{}^{209}\text{Bi}$ reaction.

It is rather surprising that, at this level of accuracy, total fusion (only three points) is not at all reproduced by the CDCC calculations based on the work in Ref. ⁴⁷ and that the ${}^6\text{He}$ induced total fusion is smaller than ${}^4\text{He}$ induced fusion *i.e.*, fusion is hindered not enhanced. However, the ${}^4\text{He}$ induced fusion at the highest energies originate from other data as stated also in Ref.⁴⁰. These points should be investigated further, experimentally and theoretically.

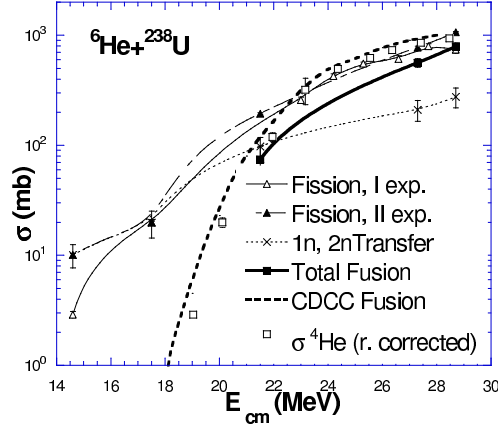


Fig. 5. Cross sections measured in the system ${}^6\text{He}+{}^{238}\text{U}$. Total fission from the first experiment (open triangles), from the second experiment (filled triangles), yields of the α -fission fragment coincidences, *i.e.*, 1n or 2n transfer induced fission (crosses), and total fusion deduced from the second experiment (filled squares). The relative theoretical fusion cross section calculated using CDCC is shown (bold-dotted curve). The cross sections for ${}^4\text{He}$ induced fusion are also reported (open squares). These last data include a small correction due to the geometrical difference between the two projectile radii. The curves connecting the various points are drawn to guide the eye.

4.1.3. The ${}^6\text{He}+{}^{64}\text{Zn}$ system

This experiment was done at the Cyclotron Research Centre in Louvain la Neuve (Belgium) using the two coupled cyclotrons via the ISOL method²¹ with $\sim 3 \times 10^6$ pps beam intensity. Four beam energies were explored in the range of 10 to 13.6 MeV ($V_B = 9.5$ (10.4) MeV in the center of mass (laboratory) system). The ${}^6\text{He}$ primary beam had the energy fixed at the maximum value and the lower energy points were obtained by a suitable number of niobium absorbers ~ 3 mg/cm² thick. The experimental set up was arranged in order to measure a) the X-rays emitted following the electron capture decay of various evaporation residues offline, and b) the ${}^6\text{He}$ scattering events and the inclusive α -particle channels originating most likely from transfer/stripping-breakup. For this second part, the large area segmented detector LEDA was utilized.⁴⁸ For comparison, the $\alpha+{}^{64}\text{Zn}$ system was measured with the same setup at three energies overlapping those of the ${}^6\text{He}+{}^{64}\text{Zn}$ system.

The main results⁴⁹ are summarized here. A strong population of the ${}^{65}\text{Zn}$ (= n+target) nucleus was observed. The cross section is much larger than the αn evaporation yield predicted by the statistical model code CASCADE⁵⁰. The cross section for the 2n(producing ${}^{68}\text{Ge}$), pn(${}^{68}\text{Ga}$), p2n(${}^{67}\text{Ga}$), and αn (${}^{65}\text{Zn}$) channels were measured. Their sum is essentially the total fusion cross section if the αn contribution is excluded, since the ${}^4\text{He}$ +target incomplete fusion produces, most likely, the same

X-ray emitters ^{67}Ge (1n evaporation) and ^{67}Ga (1p evaporation) as the ^6He +target complete fusion. This total fusion could be slightly underestimated since there could be some missing channels, like the 3n(1n) emission from $^6\text{He}(^4\text{He})$ capture, which, however, are expected to contribute a negligible amount. Still, the comparison with the $^4\text{He}+^{64}\text{Zn}$ system measured in the same way is quite meaningful.

Once the measured α n contribution is replaced by that calculated by **CASCADE**, and trivial geometric corrections are included there is no difference between ^6He and $^4\text{He}+^{64}\text{Zn}$ cross sections in the few points measured, *i.e.*, neither enhancement nor hindrance. The reaction cross sections extracted from the elastic scattering data confirm the existence of strong reaction channel(s) in addition to fusion. The potential extracted from the optical model fit to the elastic scattering data, with $r_0 = 1.2$ fm, does not reproduce the fusion cross sections with the **CCFULL**⁵¹ calculations. For a good agreement, a smaller value of $r_0 = 1.0$ fm has to be used in the calculations. But such a choice is difficult to justify on the basis of measured nuclear radii and related systematics, unless r_0 is treated simply as an adjustable parameter to reproduce experimental data. The fact that the potential extracted from the elastic scattering data does not reproduce the fusion data is not unexpected. A similar conclusion was already pointed out; see in particular Ref. ⁵². The interpretation of this is that the elastic scattering samples a different portion of the potential, more peripheral than the one involved in fusion. Therefore, this potential does not necessarily apply to the fusion process.

4.1.4. *The $^{6,8}\text{He}+^{63,65}\text{Cu}$ and $^6\text{He}+^{188,190,192}\text{Os}$*

These measurements⁵³ were performed at GANIL/SPIRAL where the radioactive beams are produced via the ISOL method.²⁰ The ^6He (^8He) beam had an intensity of 10^7 (7×10^4) pps, a beam spot on the target of 5 (8) mm in diameter, and a good resolution of 0.1% in both cases. The following energies were utilized: $^6\text{He} + ^{65}\text{Cu}$ 19.5 and 30 MeV ($V_B = 9.7$ MeV), $^6\text{He}+^{63}\text{Cu}$ 30 MeV, $^8\text{He}+^{63}\text{Cu}$ 27 MeV, and $^6\text{He}+\text{Os}$ targets 30 MeV ($V_B = 21$ MeV). The detector array consisted of 8 γ -ray clover detectors from EXOGAM located 10.5 cm from the target and an annular segmented SSD (16 rings x 16 segments) for charged particle detection positioned around 0 degrees at ~ 3.5 cm from the target. This way the system could detect in beam γ rays, forward emitted charged particles (CP), and CP- γ coincidences.

With the Cu targets the following data were obtained: the cross sections for production of various evaporation residues and/or transfer products (from the characteristic γ rays of the nuclei populated), Q-value spectra, and elastic scattering angular distributions which yielded total reaction cross sections. It should be pointed out that this is the first time that fusion cross sections induced by RIBs could be measured via in beam γ -ray techniques.

In the $^6\text{He}+^{65}\text{Cu}$ system measured at two energies, it was observed that the population of ^{66}Cu ($=1n+^{65}\text{Cu}$) is ~ 10 times stronger than the α n evaporation channel predicted by statistical model calculations. The analysis of the Q-value spectra in-

icates that ^{66}Cu is populated mainly from the $1n$ evaporation from ^{67}Cu produced by $2n+^{65}\text{Cu}$. The fusion cross section, most likely complete fusion, plus this strong transfer/stripping-breakup cross section constitute the largest amount, 85%, of the total reaction cross section deduced from the elastic scattering data. The remaining 15% is, most likely, the exclusive breakup cross section with all fragments in the exit channel. The $^4\text{He}+^{63,65}\text{Cu}$ systems were investigated in parallel at the Bombay 14UD BARC-TIFR tandem accelerator (India) via a similar in beam gamma-ray technique. In this case the strong transfer/stripping-breakup channel was absent.

The data collected with the Os targets have, in some cases, lower statistics, and for the ^{190}Os target the absolute cross sections could not be determined. Nonetheless, the Os targets results are consistent with the Cu target results.

4.1.5. Comments on the ^6He induced reactions

For the total fusion measured with ^{209}Bi , ^{238}U , and ^{64}Zn targets, only the $^6\text{He}+^{209}\text{Bi}$ system shows enhancement with respect to the ^4He total fusion, but only for the two lowest energy points. This is, for the moment, attributed to the coupling to breakup excitations, as predicted by theories. A remeasurement of these cross sections with higher statistics would be desirable. The really new and strong effects originating from the breakup process are the inclusive and exclusive alpha particle yields. The strongest channels are assigned to the formation of the systems (n +target) and ($2n$ +target). These are most likely not the conventional transfer processes, usually with moderate cross sections, but processes where unbound, highly excited states are formed in a sort of compound nucleus.

In order to search for possible common features in the ^6He induced reactions, we have plotted in Fig. 6 the following data, total reaction cross section, fusion+ $1n$ transfer/stripping-breakup cross section, total fusion cross section, and residual cross section as a function of E_{cm}/V_B with V_B computed with $r_0 = 1.56$ fm. The residual cross section is the difference between the total reaction and the fusion+ $1n$ transfer/stripping-breakup cross sections. It should account for all the processes not included in the fusion and in the $1n$ transfer/stripping-breakup which are essentially the $2n$ transfer/stripping-breakup and the exclusive breakup with all ^6He fragments in the exit channel.

Fusion and fusion+ $1n$ transfer/stripping-breakup cross sections increase continuously and smoothly with E_{cm}/V_B . This is essentially the increase of fusion cross section with rising bombarding energy. So all three systems seem to behave in a similar way in this aspect.

The scenario is somehow different for the total reaction cross sections and the related residual cross sections. The residual cross sections, according to the Zn and Bi data, have a maximum around the barrier. The actual height of this maximum, with respect to the Cu target data, is in part questionable since the authors state that the $1n$ transfer/stripping-breakup events could also originate from $1n$ evaporation from the system $2n$ +target.⁵³ A possible interpretation of this maximum is

that around the barrier the breakup phenomena are the strongest. This behavior is peculiar because it is different from the other two cross sections and deserves further investigation since this is the first time that it is observed. Anyhow, since these various cross sections were measured by different experimental methods they should be confirmed by check experiments.

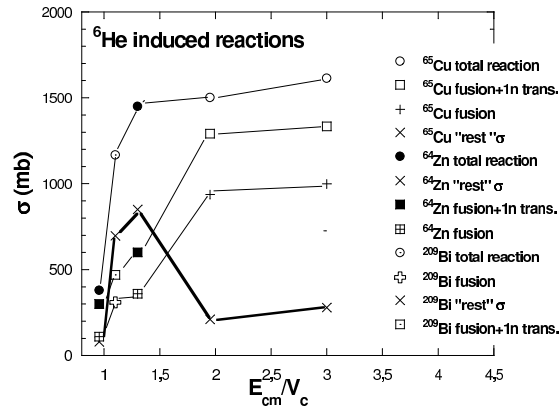


Fig. 6. Experimental cross sections for the following processes induced by ⁶He on ⁶⁵Cu, ⁶⁴Zn and ²⁰⁹Bi targets: total fusion, total fusion + 1n transfer/stripping-breakup, total reaction, and residual cross sections (labelled by “rest” in the figure). The residual cross section is the difference between the total reaction and the total fusion + 1n transfer/stripping-breakup cross sections.

4.2. ^{11,10}Be beams

These experiments were done at RIKEN in the RIBS beam line.²⁶ The ^{11,10}Be beams were produced in-flight by fragmentation of a 100 MeV/nucleon ¹³C primary beam on a thick beryllium production target. The Be beams had energy ~ 10 times larger than what is needed for fusion measurements at Coulomb barrier energies. The Be beams were, therefore, heavily degraded producing the final beam with a large energy spread, 35 to 55 MeV, and poor emittance, ~ 5 cm diameter at a ²⁰⁹Bi target. The Be beam intensities finally achieved were $>10^5$ pps. The energy of the beam particles producing fusion events were tagged event-by-event via the time-of-flight over a flight path of ~ 6 m. The detection system consisted of large area SSDs each with an active area of 5×5 cm² arranged in a compact box-like structure as close as possible to a multitarget setup. The fusion events were identified by α particles, with characteristic lifetimes and energies, emitted in the decay of the various evaporation residues populated after neutron evaporation from the compound nucleus and by the fission fragments in coincidence in two opposite SSD of the box.^{54,55} The fusion cross sections were identified as the sum of the fission

and $4n+5n$ ($3n+4n$) evaporation channels for ^{11}Be (^{10}Be). These fusion cross section could be slightly underestimated below the barrier since the $3n$ ($2n$) channel for ^{11}Be (^{10}Be) could not be measured due to its too long lifetime, $T_{1/2} = 16 \mu\text{s}$, which resulted in high random rates. Moreover, the evaporation channels with at least one charged particle, like $p\alpha n$, were not identified, since they are expected to be negligible. Even with these limitations, the comparison of ^{11}Be and ^{10}Be fusion is quite meaningful since the data were measured and analyzed in the same way. For ^{10}Be , the complete fusion cross section is taken as the total fusion because no breakup processes are realistically expected since ^{10}Be with $S_n = 6.8 \text{ MeV}$ is tightly bound. For ^{11}Be , mainly total fusion was measured since the incomplete fusion of ^{10}Be , from ^{11}Be breakup, was estimated in a previous experiment⁵⁶ to be $<30\%$ of the ^{11}Be complete fusion. These cross sections came from two independent measurements done some years apart. The statistics of the data is essentially limited by the low intensity of the radioactive beams. This causes a scattering of the various results beyond the statistical errors as discussed in detail in Ref. ^{54,55} The results are compared in the top panel of Fig. 7 as well as with the stable ^9Be beam.³²

Within the statistical accuracy of the data, the three cross sections look similar. This is astonishing since ^{10}Be is tightly bound and both ^9Be and ^{11}Be are loosely bound. In addition, the latter nucleus has a well established neutron halo structure while ^{10}Be is well bound like most of the stable nuclei. Three theoretical approaches have been followed to describe these results:

- a) CCFULL:^{54,55} The main coupling considered was the excitation of collective, rotational-like structure, with no breakup coupling.
- b) CDCC using the code FRESKO^{44,54,55} Only the two-body breakup coupling to discretized continuum states was calculated. These last calculations need several days of CPU time on modern fast PCs.
- c) coupled channel calculations using the ECIS code⁴⁰ as already mentioned in the discussion of the $^6\text{He}+^{209}\text{Bi}$ system.

The bottom panel of Fig. 7 shows the results of the first two approaches which are similar. But, if we consider also the other two beams ^{10}Be and ^9Be , the CDCC approach, particularly in the ^9Be case^{54,55} not shown in Fig. 7, underpredicts the cross sections. Apparently, the collective excitations, better handled by the CCFULL code have more strength than the breakup mode. The third approach looks, on average, worse, since it overestimates the cross section at most of the energies. But, as already pointed out, the breakup coupling is included in an indirect way via renormalization of the nuclear potential. The large collective excitation strength versus the breakup strength seems to appear also in the scattering of loosely bound ^{17}F ($S_p = 0.600 \text{ MeV}$) compared with the well bound ^{19}F (with possible collective structure), as later discussed in this review (Sect. 4.4). In the case of ^{19}F , at energies around the Coulomb barrier, the reaction cross section is larger than ^{17}F , most likely, due to a rotational-like level structure which may be excited more easily

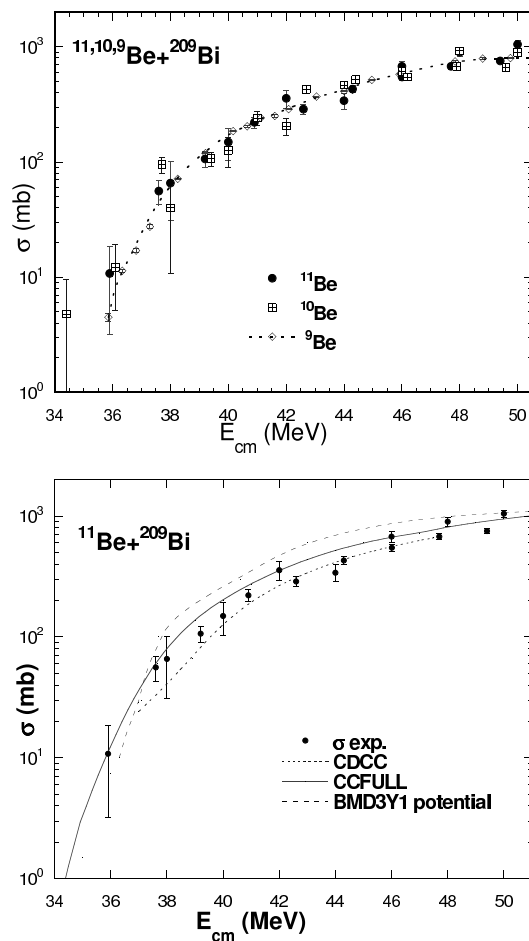


Fig. 7. Total fusion cross sections for the systems $^{9,10,11}\text{Be} + ^{209}\text{Bi}$ (top) and comparison between theories and experimental cross sections for the $^{11}\text{Be} + ^{209}\text{Bi}$ system (bottom).

than ^{17}F breakup.

For completeness, we should mention that the first attempt at GANIL to measure the $^{11}\text{Be} + ^{238}\text{U}$ system⁵⁷ leads to the successful measurement of $^6\text{He} + ^{238}\text{U}$ with the same technique.⁴⁵ The statistics were very limited so that no conclusion can be drawn from the data.

4.3. ^{11}C beam

This experiment was performed at the 88-inch cyclotron at Lawrence Berkeley National Laboratory. The system studied was $^{11}\text{C} + ^{197}\text{Au}$.⁵⁸ This experiment is worth mentioning mainly for the technique used for the production of this RIB. The

system utilized was BEARS (Berkeley Experiment with Accelerated Radioactive Species) which was based on two coupled cyclotrons. Carbon-11, $t_{1/2} = 20$ min., was produced via the $^{14}\text{N}(p,\alpha)$ reaction in a 20 atm nitrogen gas target using the cyclotron of the Biomedical Isotope Facility, located 350 m away from the 88-inch cyclotron, and then transported by a dedicated transfer line to this latter cyclotron for further acceleration. This system provided a continuous ^{11}C beam with a remarkable intensity of $1\text{-}2 \times 10^8$ pps on target. This experiment measured the excitation functions for the population of the evaporation residues, following xn evaporation from the compound nucleus. These cross sections were deduced by the yield of the α particles emitted from the ground state decay of the various At nuclei produced. The excitation functions were measured in the range of 66 to 110 MeV. The results compared with the stable ^{12}C beam are in agreement with standard evaporation model predictions by the HIVAP code⁵⁹.

4.4. ^{17}F beam

In contrast to most of the experiments discussed in the previous subsections where the interplay of neutron breakup and fusion is investigated, this subsection explores the influence of proton breakup on fusion. Fluorine-17 is a proton drip-line nucleus with a ground state binding energy of 0.600 MeV. Its first excited state is only bound by 0.105 MeV with an extended r.m.s. radius and is considered a halo state.³¹ If the ^{17}F nucleus is excited to its first excited state before fusion, the fusion cross section is expected to increase because of the lowered barrier for a larger radius. In addition, if ^{17}F breaks up prior to fusion, the core nucleus ^{16}O has a lower Z and a lower Coulomb barrier. The incomplete fusion is expected to be enhanced, too. On the other hand, as discussed in the previous section, breakup removes the ^{17}F flux available for fusion resulting in fusion suppression. Measurements of fusion of ^{17}F and ^{208}Pb was performed with the radioactive ^{17}F produced by an in-flight method using the $p(^{17}\text{O}, ^{17}\text{F})n$ reaction at ATLAS.⁶⁰ The ^{17}F beam intensity was between 1 and 2×10^5 pps with an energy resolution of about 2.5%. There was a significant ^{17}O isobar contamination in the beam with the same magnetic rigidity. The ratio of ^{17}F to ^{17}O varied with beam energies but was usually around 1. Since the energy of the ^{17}O contaminant was approximately 20% lower than that of ^{17}F , the fusion of ^{17}O with the target was estimated to contribute less than 3% to the total fusion cross section. The compound nucleus decays by fission, therefore, the fusion cross section was identified with the fission cross section. The fission fragments were detected in coincidence by four large area Si detectors. It is noted that incomplete fusion, capture of ^{16}O by the target following $^{17}\text{F} \rightarrow ^{16}\text{O}+p$ breakup, was not excluded from this measurement, so the data give the total fusion yield (CF+ICF).

The measured fusion-fission excitation function is compared to that of $^{19}\text{F}+^{208}\text{Pb}$ and $^{16}\text{O}+^{208}\text{Pb}$. No fusion enhancement was observed for ^{17}F induced fusion with respect to the stable ^{19}F and ^{16}O induced fusion on the same target. At the lowest energy of the measurement, the fusion-fission cross section is suppressed

by a factor of 4.

The breakup of ^{17}F may be a factor in influencing fusion. Measurements of ^{17}F breakup by scattering on a ^{208}Pb target were performed at energies above the Coulomb barrier (98, 120, and 170 MeV) at HRIBF (Oak Ridge National Laboratory)^{61,62,63} and below the barrier (90 MeV) at ATLAS⁶⁴. The HRIBF produced ^{17}F by the ISOL technique. The intensity was 2×10^5 pps for the first measurement and increased to 10^7 pps for subsequent measurements a year later. Since the secondary beams were accelerated by a tandem accelerator, the beam quality (energy resolution and beam spot) was as good as for stable beams. The ^{17}O isobar contaminants were removed by selecting the 9^+ charge state using an analyzing magnet. Two modes of breakup, diffraction (exclusive, two-body) and stripping (inclusive, one-body), were measured at 170 MeV. The diffraction breakup which has ^{16}O and p in the exit channel, was found to be a factor of four smaller than stripping breakup (only ^{16}O in the exit channel). This observation agrees with predictions by Esbensen.⁶² At energies near the barrier, only the stripping breakup was measured. The energy dependence of the breakup is presented along with that of fusion in Fig. 8. The stripping breakup cross sections are smaller than the fusion cross sections by factors of 4 to 10 and the diffraction breakup is four times smaller than the stripping breakup. At energies below the barrier, the diffraction breakup was studied at backward scattering angles.⁶⁴ The angle integrated breakup cross section agrees with the theoretical prediction and is very small. It is concluded that breakup of ^{17}F is weak and it has no noticeable influence on fusion.

The elastic scattering of $^{17}\text{F}+^{208}\text{Pb}$ near the barrier was analyzed by an optical model.^{63,64} Due to the thick targets used in these experiments, the energy resolution was poor. The excitation of ^{17}F to its first excited state as well as other quasielastic scattering, resulting in a small energy and/or mass change, could not be separated from the pure elastic scattering. The shape of the angular distribution for $^{17}\text{F}+^{208}\text{Pb}$ elastic scattering is similar to that of $^{16,17}\text{O}+^{208}\text{Pb}$, particularly at backward angles. These differential cross sections are much smaller than in the $^{19}\text{F}+^{208}\text{Pb}$ system. This indicates a smaller absorption cross section in the $^{19}\text{F}+^{208}\text{Pb}$. The total reaction cross sections obtained from the optical model analysis are slightly larger than the fusion cross sections, as shown in Fig. 8. The small difference between the total reaction and fusion cross sections suggests that other reaction channels such as breakup are weak and fusion enhancement is not expected. It was speculated by Romoli *et al.* that the differences in the elastic scattering between ^{17}F and ^{19}F may arise from the large collectivity of ^{19}F where the ground state is strongly coupled to its first excited state.⁶⁴ As a result, the excitation probability of ^{19}F could be significantly larger than the breakup probability of ^{17}F . Furthermore, calculations show that the excitation of ^{17}F to the first excited state is about 30% larger than the diffraction breakup.⁶⁰ Therefore, fusion following excitation to the halo state could be too small to be seen.

A large suppression of complete fusion was observed in $^9\text{Be}+^{208}\text{Pb}$ at energies above the barrier.³³ The sum of evaporation residue and fission cross sections ac-

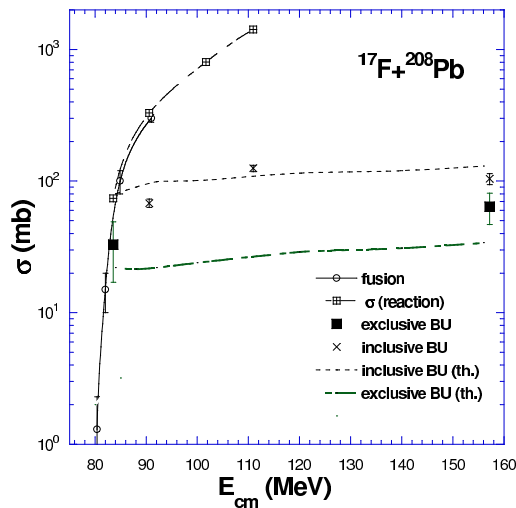


Fig. 8. The excitation function of $^{17}\text{F} + ^{208}\text{Pb}$ fusion⁶⁰ is shown by the open circles, inclusive breakup⁶³ by the crosses, and exclusive breakup⁶⁴ by the filled squares. The reaction cross sections obtained from the optical model analysis of elastic scattering data are shown by the thin dash-dotted curve. The dashed and dash-dotted curves are for stripping and diffraction breakup, respectively.⁶³

counts for 68% of the expected fusion cross section. In their measurements, the capture of a charged fragment from the breakup of ^9Be by the target (incomplete fusion) was observed. A similar situation occurs also in $^9\text{Be} + ^{209}\text{Bi}$.³² The complete and incomplete fusion make up the expected fusion cross sections. In the ^{17}F experiments, elastic scattering and breakup reaction data already exist. Further measurements of complete and incomplete fusion separately in $^{17}\text{F} + ^{208}\text{Pb}$ would be useful for a complete theoretical description of breakup and fusion.

It should be pointed out that dynamical polarization is predicted to be present when a loosely bound nucleus approaches a heavy nucleus with large Coulomb fields.^{65,66} Moreover, the dynamical polarization of a proton loosely bound nucleus will push the valence proton to the far side and get shielded from the core nucleus. This will reduce the breakup probability. In contrast, a neutron loosely bound nucleus tends to be polarized in such a way that the valence neutron lies between the core nucleus and the target which leads to large breakup cross sections. This may be the reason for low breakup cross sections for ^{17}F but large breakup cross sections for ^6He .

5. Heavy-ion reactions

In the following subsections, fusion induced by medium-mass neutron-rich radioactive nuclei is presented. This topic is of particular interests for the potential use

of neutron-rich RIBs for producing heavy elements. It is noted that for the following systems involving neutron-rich RIBs the excitation functions will be compared in reduced coordinates using the Bass model fusion barrier⁶⁷, and πR^2 with $R=1.2(A_p^{1/3}+A_t^{1/3})$, where A_p and A_t are the mass of the projectile and target, respectively, to normalize the center-of-mass reaction energy and the cross section. This is different from the procedures described in the light-ion section because the medium-mass radioactive nuclei used in experiments so far, are not very extended or loosely bound.

5.1. ^{29,31}Al beams

The radioactive Al beams were produced by fragmenting 90 MeV/nucleon ⁴⁰Ar at RIKEN. Thick Al degraders were used to decrease the secondary Al beams to the appropriate region of energy. This resulted in a very large energy spread in the beams. It was necessary to use event-by-event time-of-flight measurements to define the energy of each beam particle. They were also used in the data analysis for setting gates to remove events originating from contaminant induced reactions. The beam intensity was 1×10^5 and 3×10^4 pps for ²⁹Al and ³¹Al, respectively. To avoid changing beam energies, a stack of ten mylar backed ¹⁹⁷Au targets was placed in series along the beam direction. The excitation function was obtained in one run.⁶⁸

The compound nuclei formed in these reactions decay by fission. Therefore, the measured fission excitation function was taken as the fusion excitation function. The fission fragments were identified by two pairs of multiwire proportional counters (MWPC) placed on each side of the target stack. Valid fission events required a simultaneous detection of both fragments with the MWPCs. The target from which the fission fragments originated was identified by reconstructing the tracks of the fragments. The cross sections were scaled and checked with separate measurements using stable ²⁷Al beams.

All three excitation functions, ^{27,29,31}Al+¹⁹⁷Au, exhibit large enhancement near and below the barrier with respect to barrier penetration model predictions.⁶⁸ The enhancement cannot be accounted for by coupled-channel calculations including excitation of the projectile and target, and the static deformation of the target. Nevertheless, when the excitation functions are plotted in reduced coordinates which factor out the differences in nuclear sizes and barrier heights, they overlap each other, as shown in Fig. 9. In order to avoid the influence from coupling to the intrinsic degrees of freedom at energies near the barrier, the cross sections from high energy measurements were fitted with $\sigma = \pi R^2(1 - V_b/E)$ to extract the barrier height V_b and barrier radius R_b . It was found that the barrier height for ²⁹Al and ³¹Al induced fusion with respect to ²⁷Al was reduced by 3.4 and 4.5 MeV, and the barrier radius was decreased by 0.1 and 0.2 fm, respectively. In contrast, the Bass model⁶⁷ predicts that the reduction of barrier height and the decrease of barrier radius is 1.2 MeV and 0.2 fm for ²⁹Al induced fusion as compared to ²⁷Al induced fusion. The larger reduction in measured barrier height compared to the Bass model

prediction may be due to the large deformation in ^{27}Al .

Watanabe *et al.* fitted the excitation functions with Stelson's model assuming a flat distribution of barriers.⁶⁹ The threshold barrier for neutron flow correlates with the binding energy of the participants. The neutron binding energies are 13.1, 9.4, 7.2, and 8.1 MeV for $^{27,29,31}\text{Al}$ and ^{197}Au , respectively. The neutrons are likely to flow from Au to $^{27,29}\text{Al}$ and from ^{31}Al to Au. Although the threshold barrier height and the direction of flow are different in the three systems, the barrier thickness and the sub-barrier enhancement are very similar, which is surprising but also puzzling.⁶⁸

It is noted that the Q-value for two and four-neutron pickup in ^{27}Al and two-neutron stripping in ^{31}Al are positive. All the other neutron transfer reactions (up to four neutrons) have negative Q-values. For this reason, the fusion is not likely to be enhanced by sequential neutron transfer. This may distinguish neutron flow from neutron transfer as a mechanism that can enhance the sub-barrier fusion rate. On the other hand, the Q-values for proton stripping reactions become more positive as the Al isotopes become more neutron-rich. For instance, the Q-value is as large as 16.3 MeV for $^{197}\text{Au}(^{31}\text{Al}, ^{34}\text{S})^{194}\text{Os}$. The coupling of proton transfer reactions, which was not considered in the previous calculations, may be important in neutron-rich radioactive nuclei induced fusion.⁷⁰

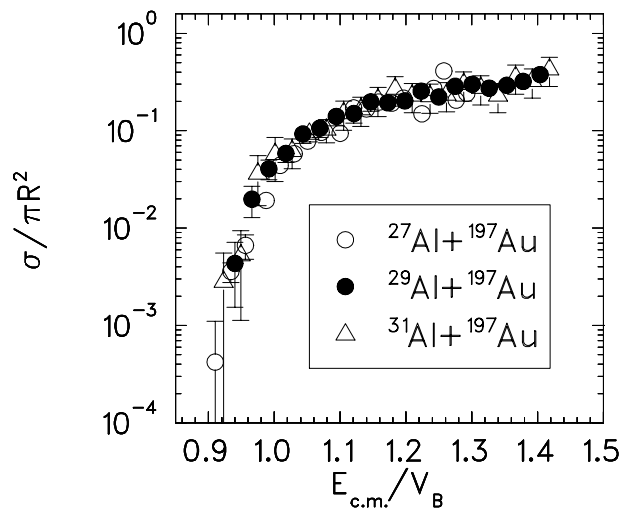


Fig. 9. Comparison of fusion excitation functions for $^{27,29,31}\text{Al}+^{197}\text{Au}$ in reduced coordinates. The open circles are for ^{27}Al induced fusion, the closed circles are for ^{29}Al , and the open triangles are for ^{31}Al .

5.2. ^{38}S beam

This experiment compares the fusion excitation function of radioactive ^{38}S on ^{181}Ta to that of stable ^{32}S on the same target.^{71,72} Since neither the sulfur isotopes nor the ^{181}Ta nucleus is magic, any effects due to the shell closure can be realistically excluded. The ^{38}S beams were produced by projectile fragmentation of a 40 MeV/nucleon ^{40}Ar beam on a ^9Be target at NSCL. The energy of the ^{38}S beam delivered to the experiment was 8 MeV/nucleon, therefore, beam degradation was necessary. This was achieved by using Al foils of various thickness mounted at the entrance of the scattering chamber to degrade the beam to the desired energies, 161.2 to 254.0 MeV. An energy spread of 2.5 MeV FWHM was observed as a result of the degradation process. The beam intensities on target ranged from 2×10^3 to 1×10^4 pps with 85% to 90% ^{38}S . Two sets of timing channel plates and parallel plate avalanche counters (PPAC) were used for event-by-event beam tracking and time-of-flight measurement. According to a statistical model prediction, more than 99% of the compound nucleus formed in this reaction decays by fission. The measured fission excitation function was taken as the fusion excitation function. The fission fragments were detected in an array of PPACs and Si detectors. A valid event was defined by fragment-fragment coincidence gated by time-of-flight associated with the ^{38}S beam. The fission cross section was normalized to the Rutherford scattering measured by a forward angle Si detector.

Quasifission usually complicates fusion-fission measurements in heavy systems. In quasifission, the interacting nuclei are captured inside the fusion barrier but fail to evolve inside the fission saddle point and re-separate. Thus the process differs from fission fragments emitted from a fully equilibrated compound nucleus. To distinguish these two processes in a low statistics RIB experiment is very difficult. Nevertheless, one-dimensional barrier penetration models and coupled-channel calculations give results for capture inside the fusion barrier which includes quasifission for heavy systems. Here, the fusion cross section actually refers to the capture cross section.

The excitation functions for ^{32}S and ^{38}S induced fusion are compared in Fig. 10 by reduced cross section and reduced energy as described in the previous section. The fusion cross sections for $^{38}\text{S}+^{181}\text{Ta}$ are generally larger than those for $^{32}\text{S}+^{181}\text{Ta}$. It is noted that the comparison is presented differently in Ref. ^{71,72} where the reduced cross section and reduced energy are calculated with the experimentally extracted barrier radius and barrier height, respectively. In that case, the two excitation functions coincide. The barrier height V_b and barrier radius R_b extracted by fitting the high energy cross sections to the classical limit $\sigma = \pi R^2(1 - V_b/E)$ show that the barrier height was reduced significantly, by 5.9 MeV, and the barrier position shifted by 1.8 fm for ^{38}S with respect to ^{32}S .⁷² According to the Bass model, the barrier height decreases by 3.4 MeV and the barrier radius increases by 0.4 fm. The larger barrier shift may be attributed to the deformation of ^{38}S ($\beta_2=0.246$)⁷³. This deformation, not accounted for in the Bass

model, may result in the difference shown between Fig. 10 (enhancement) in this paper and Fig. 4 in Ref.⁷¹ (no enhancement).

The Q-value for ^{38}S induced fusion is 6.3 MeV lower than that for ^{32}S induced fusion. The excitation energy of the compound nucleus is, therefore, 12.2 MeV lower at the barrier. As the excitation energy of the compound nucleus decreases, the total number of neutrons evaporated decreases, however, the strength of lower multiplicity neutron evaporation channels actually increases. This is a very valuable piece of information. A colder compound nucleus formed in neutron-rich radioactive nucleus induced fusion will increase the production yield of neutron-rich heavy elements.

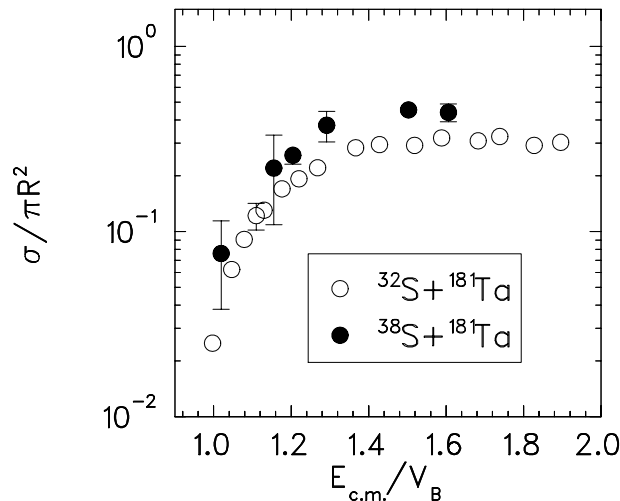


Fig. 10. Reduced fusion-fission excitation functions for $^{38}\text{S}+^{181}\text{Ta}$ (closed circles) and $^{32}\text{S}+^{181}\text{Ta}$ (open circles).

5.3. ^{132}Sn beam

The advent of accelerated ^{132}Sn for experiments is important for nuclear physics since ^{132}Sn is a doubly magic nucleus ($Z=50$, $N=82$). It has a large N/Z ratio (1.64) and has eight extra neutrons compared to the heaviest stable Sn isotope, ^{124}Sn . The fusion-evaporation excitation functions of ^{64}Ni on even Sn isotopes from $A=112$ to 124 have been measured.⁷⁴ Being able to extend the Ni+Sn systems to the very neutron-rich $^{132}\text{Sn}+^{64}\text{Ni}$ system is very exciting.

The ^{132}Sn beams were produced with the ISOL technique at the HRIBF. The short-lived ^{132}Sn ($t_{1/2} = 39.7$ s) is a product of proton induced ^{238}U fission. Since most of the mass 132 isobars produced is ^{132}Te , sulfur was introduced into the ion source to purify the beam.⁷⁵ This relies on the fact that sulfur and tin form chemical compounds at a much higher rate than other produced mass 132 isobars. The SnS^+

molecular ions were subsequently broken up in a charge exchange cell. In this way, the composition of the beam consisted of 96% ^{132}Sn . The small amount of ^{132}Te had negligible effects on the measurement because the higher Z gives a higher Coulomb barrier and fusion is, therefore, suppressed. The Sn^- ions were accelerated in the 25 MV tandem electrostatic accelerator. The average beam intensity for the experiment was 2×10^4 pps with a maximum of 5×10^4 pps. Since at energies near and below the Coulomb barrier the predominant decay mode of the compound nucleus is particle evaporation, residue cross sections were measured. This is an inverse kinematics reaction, therefore, the residues are forward focused. A combination of time-of-flight detectors and an ionization chamber placed at zero degrees provided high efficiency for residue detection. Cross sections of the order of mb can be measured.

The evaporation residue excitation function for $^{132}\text{Sn}+^{64}\text{Ni}$ is shown in Fig. 11 in reduced coordinates.⁷⁶ The cross sections for stable even Sn isotopes are shown in the same figure for comparison. As can be seen, the ^{132}Sn induced fusion is very much enhanced at sub-barrier energies. Coupled-channel calculations were performed to compare with the measured data. Since statistical model calculations predicted that fission is negligible at $E_{cm} \leq 160$ MeV, the evaporation residue cross sections are taken as fusion cross sections. Coupled-channel calculations including projectile and target excitation to their first 2^+ and 3^- states are in fair agreement with $^{64}\text{Ni}+^{124}\text{Sn}$ data but fail to reproduce $^{64}\text{Ni}+^{132}\text{Sn}$ data, as shown in Fig. 12. It is noted that $^{64}\text{Ni}+^{124}\text{Sn}$ has only one transfer channel, ($^{64}\text{Ni},^{66}\text{Ni}$), with a positive Q-value. For $^{64}\text{Ni}+^{132}\text{Sn}$, the Q-values for ^{64}Ni picking up two to six neutrons are positive. Coupled-channel calculations including inelastic excitation and transfer reactions reproduces well the $^{64}\text{Ni}+^{124}\text{Sn}$ data. But there is still large discrepancy between the calculation, shown by the solid curve in Fig. 12, and measurement for $^{64}\text{Ni}+^{132}\text{Sn}$. It should be pointed out that the form factors implemented for the multinucleon transfer⁷⁷ were extrapolated from the $^{58}\text{Ni}+^{124}\text{Sn}$ measurements.⁷⁸ Further development of the calculation and measurement of nucleon transfer are necessary for better understanding the enhancement observed here. The $^{64}\text{Ni}+^{124,132}\text{Sn}$ comparison is very similar to that of $^{40}\text{Ca}+^{90,96}\text{Zr}$.⁷⁹ There is no transfer channel with positive Q-value in $^{40}\text{Ca}+^{90}\text{Zr}$, but several neutron transfer channels with positive Q value are in $^{40}\text{Ca}+^{96}\text{Zr}$. Coupled-channel calculations considering inelastic excitation reproduce well the $^{40}\text{Ca}+^{90}\text{Zr}$ data. When inelastic excitation and transfer were coupled, the calculations underpredicted the $^{40}\text{Ca}+^{96}\text{Zr}$ data. However, only simultaneous nucleon transfer was considered in their calculations and sequential nucleon transfer may be more important.⁷⁹ Moreover, Stelson's neutron flow mechanism may play a role in $^{40}\text{Ca}+^{96}\text{Zr}$ because the barrier distribution is broader and flatter as compared to that of $^{40}\text{Ca}+^{90}\text{Zr}$. It is conceivable that the neutron flow mechanism can become more dominant than the coupling to surface modes in very neutron-rich nucleus induced fusion. When the ^{132}Sn beam intensity is greater in the future, it will be very useful to perform high precision excitation function measurements to study the barrier distributions.

In the ^{38}S and $^{29,31}\text{Al}$ experiments, no further fusion enhancement relative to

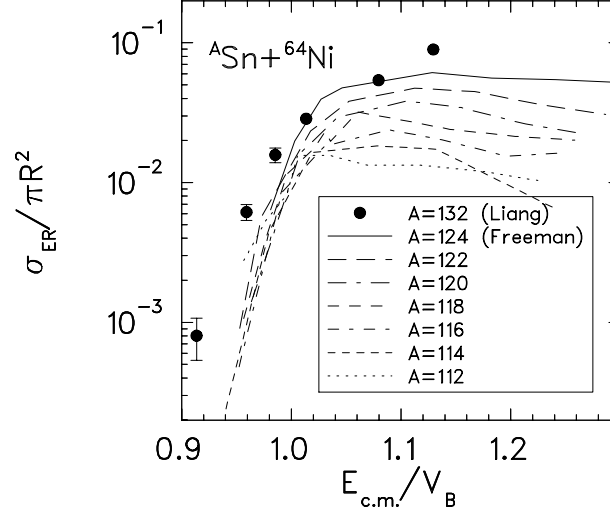


Fig. 11. Reduced evaporation residue excitation function for $^{64}\text{Ni}+^A\text{Sn}$. The filled circles are for reactions induced by ^{132}Sn .

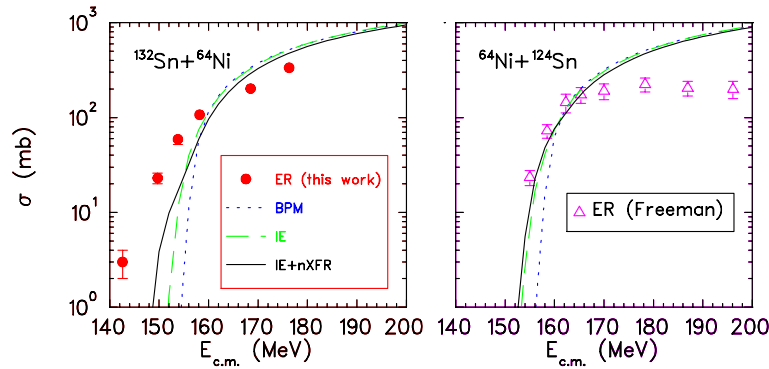


Fig. 12. Comparison of measured ER excitation functions with coupled-channel calculations. The left panel is for $^{132}\text{Sn}+^{64}\text{Ni}$ and the right panel is for $^{64}\text{Ni}+^{124}\text{Sn}$. The measured ER cross sections are shown by the filled circles and open triangles for $^{132}\text{Sn}+^{64}\text{Ni}$ and $^{64}\text{Ni}+^{124}\text{Sn}$, respectively. One-dimensional barrier penetration model prediction, coupled-channel calculations including inelastic excitation, and inelastic excitation and transfer are shown by the dotted, dashed and solid curves, respectively.

the stable isotope induced reaction was found, but large enhancement was observed in the ^{132}Sn experiment. It is noted that in the former two experiments the neutron-rich nucleus is the light reactant whereas in the latter experiment, the neutron-rich nucleus is the heavy reactant. Moreover, ^{132}Sn has eight extra neutrons compared to the heaviest stable Sn isotope whereas ^{38}S and ^{31}Al have two and four extra neutrons compared to the heaviest stable S and Al isotopes, respectively.

In fusion induced by neutron-rich nuclei such as ^{38}S , the lowering of the excitation energy can increase the cross section for lower multiplicity neutron evaporation channels. If the fusion is further enhanced as seen in the ^{132}Sn induced fusion, the cross section for lower multiplicity neutron evaporation channels can be further increased. There could be an advantage to using neutron-rich RIBs to produce heavy elements if the intensity is sufficiently high. Experiments using more neutron-rich radioactive nuclei are underway to look for systematic trends. These new experiments will provide more clues for understanding the mechanisms for fusion enhancement. As the nuclei become more neutron-rich, the neutron binding energy decreases and neutron breakup will start to play a role. Whether neutron breakup in heavy-ion reactions influences fusion the same way as light-ion reactions and the implication on heavy element production will be interesting to study.

6. Concluding Remarks

6.1. *Present situation*

From the analysis of the various results presented in this review it is clear that presently they suffer from the lack of good statistics as compared with those obtained with stable beams which are usually at least three orders of magnitude more intense. The situation will remain like this for sometime until new dedicated RIB facilities will be in operation.^{80,81,82} These first generation experimental data give still valuable results, but one should only expect to get hints from them rather than clear indications as with stable beams. For the moment, the main indications, keeping in mind the ^6He results, are that for light nuclei with loosely bound neutrons, there is not such a large sub-barrier fusion enhancement as predicted by many theories. However, there is a new effect which appears in a strong channel(s) where the light projectile fragment(s) are trapped into the target by the nuclear field in a nonconventional transfer process that could be called transfer/stripping-breakup. Such a process seems to be weaker with light projectiles when they have loosely bound protons as in ^{17}F . This different behavior could be tentatively explained by invoking different effects of the polarization potentials for the two projectiles. The details of such a process, which seem to be strongest at the barrier (see Fig. 6), have to be further investigated theoretically and experimentally.

With medium mass RIBs, no fusion enhancement is expected from the halo structure since the beams that are available today are not near the drip-lines. The relevant point could be the large neutron excess of some specific RIBs like ^{132}Sn . The data are, for the moment, quite scarce and scattered throughout the nuclear chart so it is nearly impossible to see any trend. Only for the heaviest system discussed in this paper is sub-barrier fusion enhanced. This may be attributed to the large neutron excess of the projectile, ^{132}Sn , which has eight neutrons more than the heaviest stable ^{124}Sn . It is conceivable that neutron transfer plays an important role in enhancing fusion yields. But the simplified treatment of transfer channels in the theory fails to predict such an enhancement. More systematic data focused on

specific systems will be necessary for heavy systems in order to identify a trend in fusion.

6.2. Perspectives

Nuclear reactions are often used as tools for probing nuclear structure. As more species of RIBs become available and further away from stability, fusion induced by neutron-rich radioactive nuclei could be used to explore the properties of neutron skin and neutron halo in heavier nuclei.

In very heavy reaction systems, the extra-push energy is required for complete fusion.⁸³ The extra-push energy depends on the effective fissility parameter, a measure of the Coulomb repulsion against the nuclear surface tension, of the system. How the extra-push energy affects fusion induced by very neutron-rich radioactive nuclei is an important research subject. It can provide information on whether it is practical to use such beams for producing heavy elements. Another quantity related to heavy element production is the survival probability, which correlates with the fission barrier. The systematics of fission barrier heights is obtained from stable and proton-rich nuclei⁸⁴. With shell corrections, fission barriers for neutron-rich heavy elements were predicted. The location of shell closure in very heavy nuclei may be probed by fusion studies using neutron-rich radioactive beams. To better understand the reaction dynamics, measuring evaporated particles from neutron-rich radioactive nucleus induced fusion will be useful. One can also learn about the level density of a neutron-rich compound nucleus.

It has been demonstrated that barrier distributions can be extracted from high precision fusion excitation function measurements. The distribution of barriers can reveal the signature of channel couplings. It identifies the important channels which contribute to the sub-barrier fusion enhancement. With the RIBs available today, it is not practical to perform such measurements because the intensity is orders of magnitude too low. Some proposed new RIB facilities are designed to deliver beams of intensity comparable to stable beams. These new facilities will allow the barrier distribution to be measured in a reasonable period of beam time.

While we are devoting a great deal of effort to RIB experiments, we should not neglect stable beam experiments. We have seen that the important results obtained with ${}^6,7\text{Li}$ and ${}^9\text{Be}$ shed light on the influence of breakup on fusion. As we move further away from stability, the beam intensity is expected to be much lower. Experimental apparatus will be more complicated and experiments will take longer times. Stable beams will have to be used to setup and calibrate equipment. Stable beam experiments may also provide valuable information to help us understand the results of RIB experiments which frequently suffer from poor statistics.

In the next few years, many facilities will provide more varieties of RIBs with energies above the Coulomb barrier. The projected intensity for some of the beams will reach above 10^8 pps. More fusion experiments will be performed and we expect to see some measurements with very good statistics. Reaction channels that are

important to sub-barrier fusion enhancement, such as nucleon transfer and inelastic excitation can be measured with higher intensity beams and dedicated apparatus. At the same time, experiments will push towards using beams further away from the stability. Progresses in theoretical treatment of fusion involving RIBs will be made with new experimental results. Furthermore, there are several new and powerful RIB facilities^{80,81} that are under consideration. When they become a reality, more exciting fusion experiments and results can be expected.

Acknowledgements

The authors wish to thank A. di Pietro, M. Trotta, N. Alamanos, N. Keeley, J. J. Kolata, P. E. Mueller, R. Raabe, and D. Shapira for kindly providing some of their data relevant for the preparation of this review and/or for critical reading of this manuscript. Research at the Oak Ridge National Laboratory is supported by the U.S. Department of Energy under contract DE-AC05-00OR22725 with UT-Battelle, LLC.

References

1. M. Beckerman, *Phys. Rep.* **129**, 145 (1985).
2. S. G. Steadman and M. J. Rodes-Brown, *Annu. Rev. Nucl. Part. Sci.* **36**, 649 (1986).
3. M. Beckerman, *Rep. Prog. Phys.* **51**, 1047 (1988).
4. A. B. Balantekin and N. Takigawa, *Rev. Mod. Phys.* **70**, 77 (1998).
5. M. Dasgupta, D. J. Hinde, N. Rowley, and A. M. Stefanini, *Annu. Rev. Nucl. Part. Sci.* **48**, 401 (1998).
6. M. S. Hussein, M. P. Pato, L. F. Canto, and R. Donangelo, *Phys. Rev.* **C46**, 377 (1992).
7. N. Takigawa, M. Kuratani, and H. Sagawa, *Phys. Rev.* **C47**, R2470 (1993).
8. C. H. Dasso and A. Vitturi, *Phys. Rev.* **C50**, R12 (1994).
9. C. R. Morton *et al.*, *Phys. Rev. Lett.* **72**, 4074 (1994).
10. A. M. Stefanini *et al.*, *Phys. Rev.* **C52**, R1727 (1995).
11. A. M. Stefanini *et al.*, *J. Phys.* **G23**, 1401 (1997).
12. H. Timmers *et al.*, *Phys. Lett.* **B399**, 35 (1997).
13. A. A. Sonzogni *et al.*, *Phys. Rev.* **C57**, 722 (1998).
14. V. Yu. Denisov, *Eur. Phys. J.* **A7**, 87 (2000).
15. V. I. Zagrebaev, *Phys. Rev.* **C67**, 016101(R) (2003).
16. M. S. Hussein, *Nucl. Phys.* **A531**, 192 (1991).
17. C. Signorini, *Nucl. Phys.* **A693**, 190 (2001).
18. *Proc. of the Sixth Int. Conf. on Radioactive Nuclear Beams*, ed. G. Savard, C. N. Davids, and C. J. Lister, *Nucl. Phys.* **A748**, (2005).
19. D. W. Stracener in *Proc. of Sixteenth Int. Conf. on Application of Accelerators in Research and Industry*, ed. J. L. Duggan and I. L. Morgan, (AIP, New York, 2001) p. 257.
20. A. C. C. Villari *et al.*, *Nucl. Phys.* **A693**, 465 (2001).
21. G. Rykewaert *et al.*, *Nucl. Phys.* **A701**, 323c (2002).
22. F. D. Becchetti and J. J. Kolata, in *Proc. of Fourteenth Int. Conf. on Application of Accelerators in Research and Industry*, ed. J. L. Duggan and I. L. Morgan, AIP Conf. Proc. No. 392 (AIP Press, New York, 1997), p. 369.
23. M. Y. Lee *et al.*, *Nucl. Instrum. Methods* **A422**, 536 (1999).

24. B. Harss *et al.*, *Rev. Sci. Instrum.* **71**, 380 (2000).
25. D.J. Morrissey *et al.*, *Nucl. Instrum. Methods* **B204**, 90 (2003).
26. T. Kubo *et al.*, *Nucl. Instrum. Methods* **B70**, 309 (1992).
27. I. Tanihata *et al.*, *Phys. Lett.* **B229**, 261 (1992).
28. G. D. Alkazov *et al.*, *Phys. Rev. Lett.* **78**, 2313 (1997).
29. I. Tanihata *et al.*, *Phys. Lett.* **B206**, 592 (1988).
30. M. Fukuda *et al.*, *Phys. Lett.* **B268**, 339 (1991).
31. R. Morlock *et al.*, *Phys. Rev. Lett.* **79**, 3837 (1997).
32. C. Signorini *et al.*, *Eur. Phys. J.* **A5**, 7 (1999).
33. M. Dasgupta *et al.*, *Phys. Rev. Lett.* **82**, 1395 (1999).
34. J. J. Kolata *et al.*, *Phys. Rev. Lett.* **81**, 4580 (1998).
35. E. F. Aguilera *et al.*, *Phys. Rev. Lett.* **84**, 5058 (2000).
36. E. F. Aguilera *et al.*, *Phys. Rev.* **C63**, 061603(R) (2001).
37. J. P. Bychowski *et al.*, *Phys. Lett.* **B596**, 266 (2004).
38. P. A. DeYoung *et al.*, *Phys. Rev. Lett.*, submitted.
39. C. Signorini *et al.*, *Phys. Rev.* **C67**, 044607 (2003).
40. N. Alamanos *et al.*, *Phys. Rev.* **C65**, 054606 (2002).
41. I. Raynal, *Phys. Rev.* **C23**, 2571 (1981).
42. D. T. Khoa *et al.*, *Phys. Lett.* **B342**, 6 (1995).
43. K. Rusek *et al.*, *Phys. Rev.* **C70**, 014603 (2004).
44. I. J. Thompson, *Comput. Phys. Rep.* **7**, 167 (1988).
45. M. Trotta *et al.*, *Phys. Rev. Lett.* **84**, 2342 (2000).
46. R. Raabe *et al.*, *Nature* **431**, 823 (2004).
47. K. Rusek *et al.*, *Phys. Rev.* **C67**, 41604 (2003).
48. T. Davinson *et al.*, *Nucl. Instrum. Methods* **A454**, 350(2000).
49. A. DiPietro *et al.*, *Phys. Rev.* **C69**, 044613 (2004).
50. F. Pöhlhofer, *Nucl. Phys.* **A280**, 267 (1997).
51. K. Hagino, N. Rowley, and A. T. Kruppa, *Comput. Phys. Commun.* **123**, 143 (1999).
52. J. O. Newton *et al.*, *Phys. Rev.* **C70**, 024605 (2004).
53. A. Navin *et al.*, *Phys. Rev.* **C70**, 044601 (2004).
54. C. Signorini *et al.*, *Eur. Phys. J.* **A2**, 227 (1998).
55. C. Signorini *et al.*, *Nucl. Phys.* **A735**, 329 (2004).
56. A. Yoshida *et al.*, *Phys. Lett.* **B389**, 457 (1996).
57. V. Fekou-Youmbi *et al.*, *Nucl. Instrum. Methods* **A473**, 490 (1999).
58. R. Josten *et al.*, *Phys. Rev. Lett.* **84**, 5068 (2000).
59. W. Reisdorf, *Z. Phys.* **A300**, 227 (1981).
60. K. E. Rehm *et al.*, *Phys. Rev. Lett.* **81**, 3341 (1998).
61. J. F. Liang *et al.*, *Phys. Lett.* **B491**, 23 (2000).
62. J. F. Liang *et al.*, *Phys. Rev.* **C65**, 051603 (2002).
63. J. F. Liang *et al.*, *Phys. Rev.* **C67**, 044603 (2003).
64. M. Romoli *et al.*, *Phys. Rev.* **C69**, 064614 (2004).
65. H. Esbensen and G. F. Bertsch, *Nucl. Phys.* **A600**, 37 (1996).
66. H. Esbensen and G. F. Bertsch, *Nucl. Phys.* **A706**, 383 (2002).
67. R. Bass, *Nucl. Phys.* **A231**, 45 (1974).
68. Y. X. Watanabe *et al.*, *Eur. Phys. J.* **A10**, 373 (2001).
69. P. H. Stelson *et al.*, *Phys. Rev* **C41**, 1584 (1990).
70. W. Henning, F. L. H. Wolfs, J. P. Schiffer, and K. E. Rehm, *Phys. Rev. Lett.* **58**, 318 (1987).
71. K. E. Zyromski *et al.*, *Phys. Rev.* **C55**, R562 (1997).
72. K. E. Zyromski *et al.*, *Phys. Rev.* **C63**, 024615 (2001).

73. H. Scheit *et al.*, *Phys. Rev. Lett.* **77**, 3967 (1996).
74. W. S. Freeman *et al.*, *Phys. Rev. Lett.* **50**, 1563 (1983).
75. D. W. Stracener, *Nucl. Instrum. Methods* **B204**, 42 (2003).
76. J. F. Liang *et al.*, *Phys. Rev. Lett.* **91**, 152701 (2003).
77. J. F. Liang *et al.*, *Prog. Theor. Phys. Supp.* **154**, 106 (2004).
78. C. L. Jiang *et al.*, *Phys. Rev.* **C57**, 2393 (1998).
79. H. Timmers *et al.*, *Nucl. Phys* **A633**, 421 (1998).
80. *RIA Physics White Paper*, (2000). (<http://www.ornl.gov/ria/>)
81. *The EURISOL Report*, (2003). (<http://www.ganil.fr/eurisol/>)
82. A. Goto, Y. Yano, and T. Katayama, *J. Phys. G: Nucl. Part. Phys.* **24**, 1341 (1998).
83. W. J. Swiatecki, *Phys. Scr.* **24**, 113 (1981).
84. A. J. Sierk, *Phys. Rev.* **C33**, 2039 (1986).